Effect of Geometrical Parameters of a Tethered Aerostat on Longitudinal Stability Boundaries

Rakesh Kumar and A. K. Ghosh

Nomenclature

a	Distance along balloon center line from nose to reference point, m
A	Aspect ratio
B	Buoyancy force, N
$\bar{c}$	Mean aerodynamic chord of tail, m
C_{Dc}	Tether cable drag coefficient
C_D, C_L	Drag and lift and coefficients, respectively
C_{m}	Pitching moment coefficient
d_c	Tether cable diameter, m
$D_{\max}, L$	Maximum diameter and length of the aerostat, m
F_X, F_Z	External forces acting on balloon parallel to x- and z-axes respectively, N
h_{br} or H_{br}	Component of distance from RP to COB, +ve for COB below RP, m
h_{cg} or H_{cg}	Component of distance from RP to COM of balloon, positive for COM below RP, m
h_{sr} or H_{sr}	Component of distance from RP to COM of balloon structure, +ve for COM below RP, m
I_x, I_y, I_z	Rolling, pitching and yawing moments of inertia, respectively, about balloon COM, kg-m^2
I_{xy}, I_{xz}, I_{yz}	Products of inertia in *XY*-, *XZ*- and *YZ*-plane respectively, kg-m^2
k_{xx}, k_{yy}, ik_{zz}	Tether force per unit displacement in x-, y- and z-axis, respectively, at BCP, N/m

R. Kumar (✉)
Aerospace Engineering Department, PEC, Chandigarh, India
e-mail: rakesh@pec.edu.in

A. K. Ghosh
Department of Aerospace Engineering, IIT, Kanpur, India

D. Shukla (ed.), *Lighter Than Air Systems*, Lecture Notes in Mechanical Engineering,
https://doi.org/10.1007/978-981-19-6049-9_1

k_{xz}, k_{zx}	Tether *x*-force per unit of *z*-displacement at BCP and vice versa, N/m
$k_{x\theta}$, $k_{z\theta}$	Tether *x*- and *y*-force per unit of pitch displacement respectively N/rad
$k_{y\varphi}$, $k_{y\psi}$	Tether *y*-force per unit of roll and yaw displacement, respectively, N/rad
$k_{\theta x}$, $k_{\theta z}$	Tether pitching moment per unit of *x*- and *y*-displacement, N-m/m
$k_{\theta\theta}$, $k_{\varphi\varphi}$, $k_{\psi\psi}$	Total tether pitch, roll and yaw moment per unit of pitch, roll and yaw displacement, respectively, about COM, N-m/rad
$k_{\theta\theta D}$, $k_{\theta\theta T}$	$K_{\theta\theta}$ Due to displacement and rotation of balloon relative to steady tension vector at BCP, N-m/rad
$k_{\varphi y}$, $k_{\psi y}$	Tether rolling and yawing moment per unit of y-displacement, Nm/m
$k_{\varphi\psi}$, $k_{\psi\varphi}$	Tether rolling moment per unit of yaw displacement and vice versa, N-m/rad
l	Tether cable length, m
l_{br} or L_{br}	Component of distance from RP to COB, positive for COB ahead of RP, m
l_{cg} or L_{cg}	Component of distance from RP to COM of balloon, positive for COM forward of RP, m
l_{sr} or L_{sr}	Component of distance from RP to COM of balloon structure, positive for COM aft of RP, m
l_{tr} or L_{tr}	Component of distance from RP to BCP, positive for BCP forward of RP, m
L_{PHT}	Distance of CG from MAC of PHT of balloon, m
m_a	Apparent mass of air associated with accelerations of balloon, kg
m_g	Mass of inflation gas, kg
m_s	Balloon structural mass (including bridle, test instr. and payload), kg
m_T	Combined mass of balloon structure and inflation gas, $\mathrm{m_g + m_s}$, kg
n	Cable drag per unit length for cable normal to the wind, N/m
S_{ref}, S_{exposed}	Reference area ($\pi D_{\max}{}^2/4$) and exposed planform area of aerostat, m^2
t_{tr} or T_{tr}	Component of distance from RP to BCP, positive for BCP below RP, m
t	Time in seconds
T, T_0, T_1	Tether cable tension, tension at lower and upper ends, respectively, N
u, w	Perturbation velocities of balloon COM along *X*- and *Z*-axes, respectively, m/s
V_∞	Steady wind velocity, m/s
V_n	Component of wind velocity normal to cable, V_∞ sin γ, m/s
W_s	Structural weight of balloon (including bridle, payload and test instrument), N
w_c	Tether cable weight per unit length, N/m
x_t, z_t	Distance parallel to *X*- and& *Z*-axis from RP to COM, +ve for COM forward and below RP, respectively

x_1, z_1	Coordinates of balloon COM with respect to tether cable anchor point, m
α	Perturbation angle of attack, rad
ϵ	Downwash angle, rad
Λ	Tail sweep angle, rad
γ_0, γ_1	Angle between horizontal and tether cable at lower and upper end, respectively, rad
ε	Angle between principal X-axis of balloon and stability axis, rad
η	Real part of characteristic root of stab. equation, damping, s^{-1}
θ	Pitch angle, rad
λ	Characteristic root of stability equations ($\eta \pm i\omega$) and taper ratio
ρ	Atmospheric density, kg/m^3
ω	Imaginary part of characteristic root of stability equations, frequency, rad/s

Subscripts

A, B, C, G	Aerodynamic, buoyancy, tether cable and gravity force terms, respectively.
t	Equilibrium trim condition
0, 1	Lower and upper end of tether cable
$\alpha, \dot{\alpha}$	With respect to α and $\dot{\alpha}\bar{c}/2V_\infty$, respectively
q, r	With respect to $q\bar{c}/2\ V_\infty$

Abbreviations

BCP, RP	Bridle confluence point and reference point
CG, COB	Center of gravity and center of Buoyancy
COM, SCM	Balloon center of mass and balloon structural center of mass
PHT	Projected horizontal tail
MAC	Mean aerodynamic chord

1 Introduction

The paper presents a systematic approach for longitudinal stability analysis and parametric study on longitudinal stability boundaries of an aerostat tethered from an earth-fixed anchor point and flying in steady wind conditions. Pant et al. [1–3] have reported good amount of research work on sizing, design and fabrication of

Aerostats. Rajani et al. [4, 5] have analyzed dynamic stability of a tethered aerostat. Worth noting work has been reported in the reports available on analytical and experimental determination of stability parameters along with trend study of balloon tethered in wind [6–8]. Authors [9, 10] have analyzed stability along with parametric trend study of a tethered aerostat. The contributions in the area of stability analysis of aerostat [11–14] and tether cable stability and dynamics [15–17] have also been reported earlier. Few references [18–20] have been used for determining some stability parameters. The paper presents mathematical modeling [8] (Sect. 2), estimation of stability characteristics (Sect. 3) and parametric trend study (Sect. 4) showing the effect of various geometrical parameters on longitudinal stability boundaries of a tethered aerostat.

2 Mathematical Modeling

The stability analysis of an aerostat tethered from an earth-fixed anchor point has been carried out under steady wind conditions. The formulations given by Redd et al. [8] have been used for mathematical modeling of the considered aerostat (Fig. 1) tethered in the steady wind conditions.

Figure 2 presents the geometrical parameters and various forces and moments acting on tethered aerostat. The use of theoretical formulations [8] based on considered aerostat configuration was made for the calculation of stability derivatives and analysis.

Figure 3 shows the coordinate system along with forces and moments used for the derivation of equations of motion of the tethered aerostat. Figure 3 also shows tether cable forces at the lower and upper end along with related angles.

Table 1 presents the geometric, mass, inertia and aerodynamic characteristics of the considered aerostat used to carry out the stability analysis. Some dimensional parameters were given, while the others were calculated for the given configuration of the tethered aerostat based on the theoretical formulations [8, 19, 20].

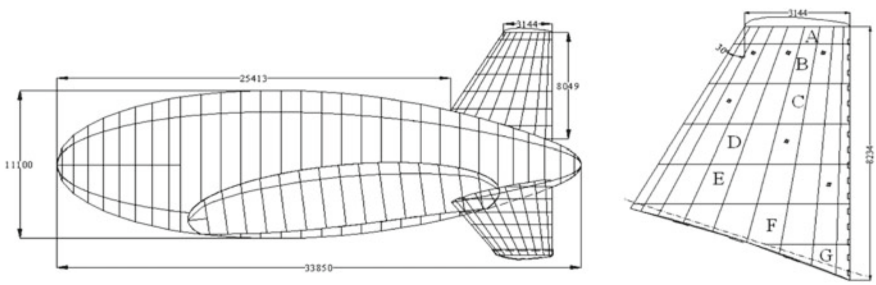

Fig. 1 Dimensions of the aerostat and fin

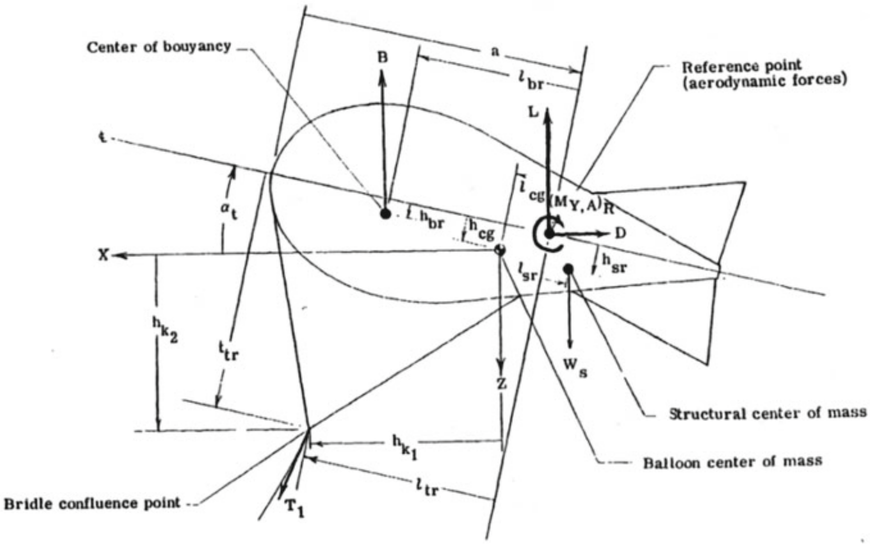

Fig. 2 Geometry of the balloon system [8]

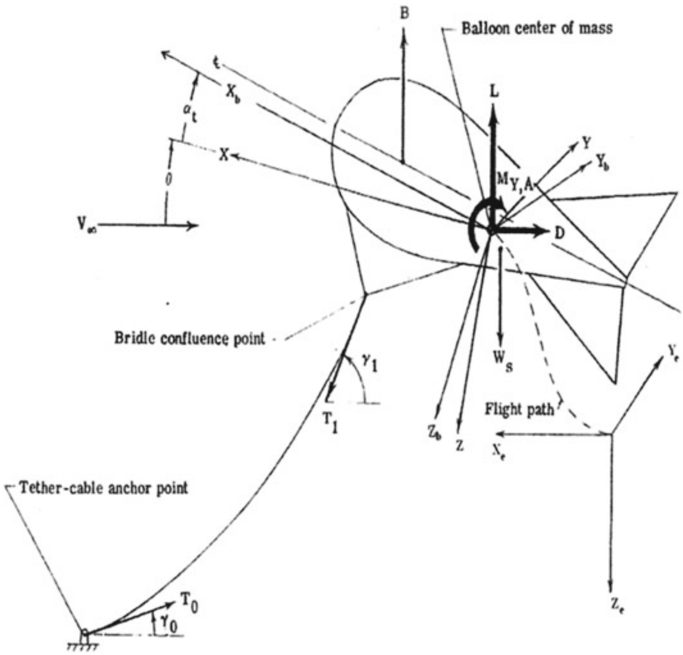

Fig. 3 Coordinate system and forces acting on tethered aerostat [8]

Table 1 Characteristics of the considered aerostat

Parameter (units)	Value	Parameter (units)	Value	Parameter (units)	Value
L_{tr} (m)	5.98	ρ_a (kg-m^{-3})	1.09	bVT (m)	8.1415
T_{tr} (m)	10.9	ρ_{he} (kg-m^{-3})	0.1759	bPVT (m)	5.7572
L_{cg} (m)	−1.92	m_T (kg)	1406	bPHT (m)	11.5145
H_{cg} (m)	0.68	m_{he} (kg)	355.85	SVT (m^2)	44.729
L_{br} (m)	0.31	m_s (kg)	1050.15	SPVT (m^2)	31.63
H_{br} (m)	0.0	$m_{x,a}$ (kg)	488.25	SPHT (m^2)	63.26
L_{sr} (m)	−3.6	$m_{y,a}$ (kg)	2283.6	S_{ref} (m^2)	96.769
H_{sr} (m)	2.4	$m_{z,a}$ (kg)	2283.6	AVT	1.482
l (m)	1000	I_{xx} (kg-m^2)	15,081.44	APVT	1.048
d_c (m)	0.017	I_{yy} (kg-m^2)	150,814.4	APHT	2.096
D_{max} (m)	11.1	I_{zz} (kg-m^2)	150,814.4	LVT (m)	4.2387
L (m)	33.85	B (N)	18,354.51	LPVT (m)	1.4795
c_t (m)	3.144	w_c (N/m)	2.943	LPHT (m)	9.4407
c_r (m)	7.844	C_{Dc}	1.17		
$\bar{c}$ (m)	5.829	λ	0.4		

The motion of the tethered aerostat consists of small perturbations about steady flight reference conditions. A linearized analysis similar to that of a rigid airplane has been used during the mathematical modeling while taking into account the following considerations.

1. The equations of motion are referred to center of mass of the balloon.
2. The balloon is symmetric laterally and has yaw, roll and side slip angles equal to zero in the reference steady-state trimmed condition (ψ_t, φ_t, $\beta_t = 0$).
3. The balloon and bridle form a rigid system.
4. The tether cable is flexible, but inextensible and contributes static forces at the bridle confluence point (BCP).
5. The cable weight and drag normal to the cable are needed only for determining the static cable forces, equilibrium shape of the cable and the cable derivatives.

Four different sources of external forces and moments such as aerodynamic, buoyant, tether cable and gravity act on a tethered aerostat. Therefore, the equations of motion of a tethered aerostat can be written as [8].

$$F_{X,A} + F_{X,C} + F_{X,B} + F_{X,G} = m_{x,o}\ddot{x}_e \tag{1a}$$

$$F_{Z,A} + F_{Z,C} + F_{Z,B} + F_{Z,G} = m_{z,o}\ddot{z}_e \tag{1b}$$

$$M_{Y,A} + M_{Y,C} + M_{Y,B} + M_{Y,G} = Iy\ddot{\theta} \tag{1c}$$

The terms $m_{x,o}$, $m_{y,o}$ and $m_{z,o}$ are total aerostat masses in x-, y- and z-directions, respectively, and can be expressed as:

$$m_{x,o} = m_s + m_g + m_{a1} \tag{2a}$$

$$m_{z,o} = m_s + m_g + m_{a3} \tag{2b}$$

The terms m_s, and m_g are the structural mass of aerostat and mass of the gas inside the aerostat. The terms m_{a1} and m_{a3} are apparent masses associated with accelerations in x- and z-directions, respectively. The apparent masses which depend upon the equilibrium trim angle of attack (α_t) are given by the following equations [8].

$$m_{a1} = m_{x,a}\cos^2\alpha_t + m_{z,a}\sin^2\alpha_t, \tag{3a}$$

$$m_{a3} = m_{x,a}\sin^2\alpha_t + m_{z,a}\cos^2\alpha_t \tag{3b}$$

The terms $m_{x,a}$ and $m_{z,a}$ are the apparent masses of the balloon accelerating along the X_b- and Z_b-axes. The mass moments of inertia which depend upon the orientation of the balloon are expressed by the following equations [8].

$$I_x = I_{xx}\cos^2\varepsilon + I_{zz}\sin^2\varepsilon \tag{4a}$$

$$I_y = I_{yy} \tag{4b}$$

$$I_z = I_{xx}\sin^2\varepsilon + I_{zz}\cos^2\varepsilon \tag{4c}$$

$$I_{xz} = \tfrac{1}{2}(I_{xx} - I_{zz})\sin^2\varepsilon \tag{4d}$$

The terms I_{xx}, I_{yy} and I_{zz} are the mass moments of inertia about the principal axes, and ε is the angle between the principal X-axis and the stability X-axis. In the present analysis, X_b-, Y_b- and Z_b-axes are considered to be principal axes; hence, $\varepsilon = \alpha_t$.

2.1 Aerodynamic Forces and Moments

The aerodynamic forces and moments at trim conditions in non-dimensional form while neglecting higher order perturbation terms are represented by the following relationships [8].

$$F_{X,A} = -\left[\left(\frac{\rho V_\infty S}{2}\right)\left(2C_D + C_{D_u}\right)\dot{x}_e\right] - \left[\left(\frac{\rho V_\infty S}{2}\right)\left(C_{D_\alpha} - C_L\right)\right]\dot{z}_e$$
$$- \left[\left(\frac{\rho V_\infty^2 S}{2}\right)\left(C_{D_\alpha} - C_L\right)\right]\theta - \left(\frac{\rho V_\infty^2 S}{2}\right)C_D \tag{5a}$$

$$F_{Z,A} = -\left[\left(\frac{\rho V_\infty S}{2}\right)\left(2C_L + C_{L_u}\right)\right]\dot{x}_e - \left[\left(\frac{\rho S\overline{c}}{4}\right)C_{L_{\dot{\alpha}}}\right]\ddot{z}_e$$
$$- \left[\left(\frac{\rho V_\infty S}{2}\right)\left(C_{L_\alpha} + C_D\right)\right]\dot{z}_e - \left[\frac{\rho V_\infty S\overline{c}}{4}\left(C_{L_{\dot{\alpha}}} + C_{L_q}\right)\right]\dot{\theta}$$
$$- \left[\frac{\rho V_\infty^2 S}{2}\left(C_{L_\alpha} + C_D\right)\right]\theta + \frac{\rho V_\infty^2 S}{2}C_L \tag{5b}$$

$$M_{Y,A} = \left[\frac{\rho V_\infty S\overline{c}}{2}\left(2C_m + C_{m_u}\right)\right]\dot{x}_e + \left[\frac{\rho S(\overline{c})^2}{4}C_{m_{\dot{\alpha}}}\right]\ddot{z}_e + \left(\frac{\rho V_\infty S\overline{c}}{2}C_{m_\alpha}\right)\dot{z}_e$$
$$+ \frac{\rho V_\infty S(\overline{c})^2}{4}\left(C_{m_{\dot{\alpha}}} + C_{m_q}\right)\dot{\theta} + \left(\frac{\rho V_\infty^2 S\overline{c}}{2}C_{m_\alpha}\right)\theta + \frac{\rho V_\infty^2 S\overline{c}}{2}C_m \tag{5c}$$

2.2 *Tether Cable Forces and Moments*

The tether cable forces and moments are expressed as [16]:

$$F_{X,C} = -k_{xx}x_e - k_{xz}z_e - (k_{x\theta} + T_1\sin\gamma_1)\theta + T_1\cos\gamma_1 \tag{6a}$$

$$F_{Z,C} = -k_{zx}x_e - k_{zz}z_e + \left(T_1\cos\gamma_1 + k_{y\theta}\right)\theta + T_1\sin\gamma_1 \tag{6b}$$

$$M_{Y,C} = -k_{\theta x}x_e - k_{\theta z}z_e - k_{\theta\theta}\theta - h_{k_1}T_1\sin\gamma_1 + h_{k_2}T_1\cos\gamma_1 \tag{6c}$$

where

$$h_{k_1} = \left(\mathrm{l}_{tr} - \mathrm{l}_{cg}\right)\cos\alpha_t + \left(t_{tr} - h_{cg}\right)\sin\alpha_t$$

$$h_{k_2} = \left(t_{tr} - h_{cg}\right)\cos\alpha_t - \left(\mathrm{l}_{tr} - \mathrm{l}_{cg}\right)\sin\alpha_t,$$

$$k_{x\theta} = h_{k_2}k_{xx} - h_{k_1}k_{x2}, \qquad k_{z\theta} = h_{k_2}k_{zx} - h_{k_1}k_{zz}$$

$$k_{\theta x} = h_{k_2}k_{xx} - h_{k_1}k_{zx}, \qquad \mathrm{k}_{\theta z} = h_{k_2}k_{xz} - h_{k_1}k_{zz}$$

$$k_{\theta\theta} = k_{\theta\theta_D} + k_{\theta\theta_T}$$

$$k_{\theta\theta_D} = h_{k_2}^2 k_{xx} - h_{k_2} h_{k_1}(k_{xz} + k_{zx}) + h_{k_1}^2 k_{zz}$$

$$k_{\theta\theta_T} = h_{k_2}(T_1 \sin\gamma_1) + h_{k_1}(T_1 \cos\gamma_1)$$

$$k_{y\varphi} = -h_{k_2} k_{yy}, \quad k_{y\psi} = h_{k_1} k_{yy}, \quad k_{\varphi y} = k_{y\varphi}$$

$$k_{\varphi\varphi} = h_{k_2}^2 k_{yy}, \qquad k_{\psi\psi} = h_{k_1}^2 k_{yy}$$

$$k_{\varphi\psi} = -h_{k_1} h_{k_2} k_{yy}, \quad k_{\psi y} = k_{y\psi}, \quad k_{\psi\varphi} = k_{\varphi\psi}$$

2.3 Buoyancy Forces and Moments

The expressions for the buoyancy forces and moments about the center of mass in the stability axis system can be expressed assuming small perturbation angles as [16]:

$$F_{X,B} = B\theta \tag{7a}$$

$$F_{Z,B} = -B \tag{7b}$$

$$\begin{aligned} M_{Y,B} = {} & B\left[\left(\mathrm{l}_{br} - \mathrm{l}_{cg}\right)\cos\alpha_t - \left(h_{cg} - h_{br}\right)\sin\alpha_t\right] \\ & - B\left[\left(h_{cg} - h_{br}\right)\cos\alpha_t + \left(\mathrm{l}_{br} - \mathrm{l}_{cg}\right)\sin\alpha_t\right]\theta \end{aligned} \tag{7c}$$

2.4 Gravity Forces and Moments

The component due to structural weight of balloon is considered during the formulation of equations of motion for gravity forces. The effects of apparent mass and lifting gas are already included in the coefficients of the acceleration and buoyancy terms, respectively. The forces and moments due to gravity for small perturbation angles are determined by [8]:

$$F_{X,G} = -W_s\theta \tag{8a}$$

$$F_{Z,G} = -W_s \tag{8b}$$

$$\begin{aligned} M_{Y,G} = {} & W_S\big[\big(\mathrm{l}_{sr} + \mathrm{l}_{cg}\big)\cos\alpha_t - \big(h_{sr} - h_{cg}\big)\sin\alpha_t\big] \\ & - W_S\big[\big(h_{sr} - h_{cg}\big)\cos\alpha_t + \big(\mathrm{l}_{sr} + \mathrm{l}_{cg}\big)\sin\alpha_t\big]\theta \end{aligned} \tag{8c}$$

3 Estimation of the Stability Characteristics

After the mathematical modeling, the stability characteristics (roots/eigen values) of the considered aerostat can be estimated by executing the following steps:

1. Calculate the trim angle of attack.
2. Obtain the aerodynamic parameters dependent on trim angle of attack for the steady-state trim condition.
3. Calculate the value of tensions in the cable at the upper and lower ends.
4. Use the value of tensions to obtain tether cable derivatives.
5. Obtain the stability equations by putting the equilibrium part of the balloon's equations of motion to zero.
6. Convert the above stability equations in the matrix form and obtain the roots/eigen values by using the results obtained in the steps 1 to 4.

3.1 Balloon Equations of Motion

After combining all the expressions for each of the external forces and moments (such as aerodynamic, buoyancy, cable-tether and gravity), the following resulting equations of motion (16) about the balloon COM can be obtained.

***X*-Force**

$$\begin{aligned} m_x\ddot{x}_e &+ \left[\frac{\rho V_\infty S}{2}\big(2C_D + C_{D_u}\big)\right]\dot{x}_e + k_{xx}x_e + \left[\frac{\rho V_\infty S}{2}\big(C_{D_\alpha} - C_L\big)\right]\dot{z}_e + k_{xz}z_e \\ &+ \left[k_{x\theta} + \frac{\rho V_\infty^2 S}{2}\big(C_{D_\alpha} - C_L\big) - (B - W_s) + T_1\sin\gamma_1\right]\theta + \frac{\rho V_\infty^2 S}{2}C_D \\ &- T_1\cos\gamma_1 = 0 \end{aligned} \tag{9a}$$

***Z*-Force**

$$\begin{aligned} m_z\ddot{z}_e &+ \frac{\rho V_\infty S}{2}\big(2C_L + C_{L_u}\big)\dot{x}_e + k_{zx}x_e + \frac{\rho V_\infty S}{2}\big(C_{L_\alpha} + C_D\big)\dot{z}_e + k_{zz}z_e \\ &+ \frac{\rho V_\infty S\bar{c}}{4}\big(C_{L_{\dot{\alpha}}} + C_{L_q}\big)\dot{\theta} + \left(k_{z\theta} + \frac{\rho V_\infty^2 S}{2}\big(C_{L_\alpha} + C_D\big) - T_1\cos\gamma_1\right)\theta \end{aligned}$$

$$+\frac{\rho V_\infty^2 S}{2}C_L + B + W_S - T_1 \sin\gamma_1 = 0 \tag{9b}$$

Pitching Moment

$$\begin{aligned}
&-\left[\frac{\rho V_\infty S\overline{c}}{2}\left(2C_m + C_{m_u}\right)\right]\dot{x}_e + k_{\theta x}x_e - \left[\frac{\rho S\overline{c}^2}{4}C_{m_{\dot\alpha}}\right]\ddot{z}_e \\
&-\left(\frac{\rho V_\infty S\overline{c}}{2}C_{m_\alpha}\right)\dot{z}_e + k_{\theta z}z_e + I_y\ddot{\theta} - \left[\frac{\rho V_\infty S\overline{c}^2}{4}\left(C_{m_{\dot\alpha}} + C_{m_q}\right)\right]\dot{\theta} \\
&+\left(k_{\theta\theta} + M_{s_1} - \frac{\rho V_\infty^2 S\overline{c}}{2}C_{m_\alpha}\right)\theta - \frac{\rho V_\infty^2 S\overline{c}}{2}C_m + h_{k_1}T_1\sin\gamma_1 \\
&-h_{k_2}T_1\cos\gamma_1 - M_{s_2} = 0
\end{aligned} \tag{9c}$$

$$\begin{aligned}
M_{s_1} &= \left[\left(\mathrm{l}_{br} - \mathrm{l}_{cg}\right)B + \left(\mathrm{l}_{sr} + \mathrm{l}_{cg}\right)W_s\right]\sin\alpha_t \\
&\quad + \left[\left(h_{cg} - h_{br}\right)B + \left(h_{sr} - h_{cg}\right)W_s\right]\cos\alpha_t \\
M_{s_2} &= \left[\left(\mathrm{l}_{br} - \mathrm{l}_{cg}\right)B + \left(\mathrm{l}_{sr} + \mathrm{l}_{cg}\right)W_s\right]\cos\alpha_t \\
&\quad - \left[\left(h_{cg} - h_{br}\right)B + \left(h_{sr} - h_{cg}\right)W_s\right]\sin\alpha_t \\
m_x &= m_{x,o} \quad \text{and} \quad m_z = m_{z,o} + \frac{\rho S\overline{c}}{4}C_{L_{\dot\alpha}}
\end{aligned}$$

3.2 *Equilibrium Trim Conditions*

In the mathematical model used for calculating the stability characteristic, it is seen that all the aerodynamic parameters are dependent on the angle of attack and it is required to calculate the angle of attack at which the steady-state trimmed condition for the balloon is achieved, this angle of attack is called the trim angle of attack. The steady-state trimmed conditions can be obtained by setting the perturbation quantities of Eq. (9a–9c) equal to zero.

$$\frac{\rho V_\infty^2 S}{2}C_D - T_1\cos\gamma_1 = 0 \tag{10a}$$

$$\frac{\rho V_\infty^2 S}{2}C_L + B - W_s - T_1\sin\gamma_1 = 0 \tag{10b}$$

$$-\frac{\rho V_\infty^2 S\tau}{2}C_m + h_{k_1}T_1\sin\gamma_1 - h_{k_2}T_1\cos\gamma_1 - M_{s_2} = 0 \tag{10c}$$

Substitute Eq. (10a–10b) into Eq. (10c) to eliminate the cable tension and angle to obtain the following trim equation:

$$h_{k_1}\left(\frac{\rho V_\infty^2 S}{2}C_L + B - W_s\right) - h_{k_2}\left(\frac{\rho V_\infty^2 S}{2}C_D\right) - \frac{\rho V_\infty^2 S\tau}{2}C_m - M_{s_2} = 0 \quad (11)$$

Equation (11) can be solved by Newton iterations to find the equilibrium trim angle of attack (α_t) for various wind velocities, provided the aerodynamic coefficients C_L, C_D and C_m are known functions. The calculated α_t can be used to solve the Eq. (10a–10c) to find and followed by the evaluation of α-dependent stability coefficients.

3.3 *Formulations for Calculation of Stability Derivatives*

The expressions for the longitudinal stability coefficient/derivatives calculated in the previous step are based on the theoretical formulation corresponding to CG location. The derivative based on the aerostat configuration has been calculated for projected horizontal (PHT). Lift curve slope expression given in Eq. (12) uses the values of constants of the respective tail (PHT).

$$C_{L_{\alpha_t}} = \frac{(2\pi A)}{\left(2 + \sqrt{4 + \frac{A^2\beta^2}{\eta^2}\left(1 + \frac{\tan^2\Lambda}{\beta^2}\right)}\right)} * \frac{S_{\text{exposed}}}{S_{\text{ref}}} \quad (12)$$

where $C_{L_{\alpha_t}}$ is the lift curve slope of the tail.

Longitudinal Derivatives (PHT).

$$C_L = 0.0061 + 1.2\alpha + C_{L_{\alpha_t}}\alpha + \eta C_{D_c}\frac{S_P}{S_{\text{ref}}}\alpha^2$$

$$C_{L_\alpha} = 1.2 + C_{L_{\alpha_t}} + 2\eta C_{D_c}\frac{S_P}{S_{\text{ref}}}\alpha$$

$$C_{L_{\dot\alpha}} = C_{L_q}\frac{\mathrm{d}\in}{\mathrm{d}\alpha}$$

$$C_{L_q} = 2C_{L_{\alpha_t}}\frac{L_{\text{PHT}}}{D}$$

$$C_D = 0.0396 + \frac{C_L^2}{\pi e \mathrm{A}}$$

$$C_{D_\alpha} = 2\frac{C_L}{\pi e A}C_{L_\alpha}$$

$$C_m = -0.02 + 0.04832\alpha + \eta C_{L_{\alpha_t}}\left(1 - \frac{\mathrm{d}e}{\mathrm{d}\alpha}\right)\frac{L_{\mathrm{PHT}}}{D}\alpha$$

$$C_{m_\alpha} = 0.048326 + \eta C_{L_{\alpha_t}}\left(1 - \frac{\mathrm{d}e}{\mathrm{d}\alpha}\right)\frac{L_{\mathrm{PHT}}}{D}\alpha$$

$$C_{m_q} = -2C_{L_{\alpha_t}}\left(\frac{L_{\mathrm{PHT}}}{D}\right)^2$$

$$C_{m_{\dot\alpha}} = C_{m_q}\tau\frac{\mathrm{d}\in}{\mathrm{d}\alpha}$$

where $\tau = \left(\frac{V_t}{V}\right)^2$.

3.4 Equilibrium Cable Shape

The forces acting on tether cable of length, l (Fig. 4) are the tension, cable weight and drag normal to the cable. Drag along the cable has been neglected. The normal drag force per unit length depends on the component of wind velocity normal to the cable V_n, the drag cable coefficient C_{D_c} and cable diameter $\mathrm{d_c}$ and can be expressed as [8]:

$$n = C_{D_c} d_c \frac{1}{2}\rho V_n^2 \tag{13}$$

Tension (T_1) at upper end of the cable using tension $\left[\frac{\mathrm{d}T}{T} = -\frac{\overline{p}}{\mathrm{q}}\left(\frac{\mathrm{d}f}{\overline{q}+\overline{p}-f} + \frac{\mathrm{d}f}{\overline{q}-\overline{p}+f}\right)\right]$ is given by

$$T_1 = T_{\tau 1/\tau} \tag{14}$$

where $\tau(\gamma) = \left(\frac{\overline{q}+\overline{p}-\cos\gamma}{\overline{q}-\overline{p}+\cos\gamma}\right)^{\frac{\overline{p}}{\overline{q}}}$, $\overline{p} = \frac{w_c}{2n}$, $\overline{q} = \sqrt{1+(\overline{p})^2}$, $f = \cos\gamma$.

For the known parameters such as $l\left(\mathrm{d}l = \left(\frac{T_1}{n\tau_1}\right)\frac{\tau}{(\sin^2\gamma + 2\overline{p}\cos\gamma)}\mathrm{d}\gamma\right)$, n, w_c, T_1 and γ_1, the following expressions can be used to determine the coordinates T_1 and γ_1 at upper end and T_0 and γ_0 at the lower end.

$$\overline{\lambda}_0 = \overline{\lambda}_1 - \frac{n\tau_1 1}{T_1} \quad \text{and} \quad T_0 = T_{1\tau 0/\tau 1} \tag{15}$$

$$\tilde{x}_1 = \frac{T_1}{n\tau_1}\int_{\gamma_0}^{\gamma_1}\frac{\tau\cos\gamma}{(\sin^2\gamma + 2\overline{p}\cos\gamma)}\mathrm{d}\gamma \quad \text{where} \quad \mathrm{d}\sigma = \frac{\tau\cos\gamma}{(\sin^2\gamma + 2\overline{p}\cos\gamma)}\mathrm{d}\gamma \tag{16}$$

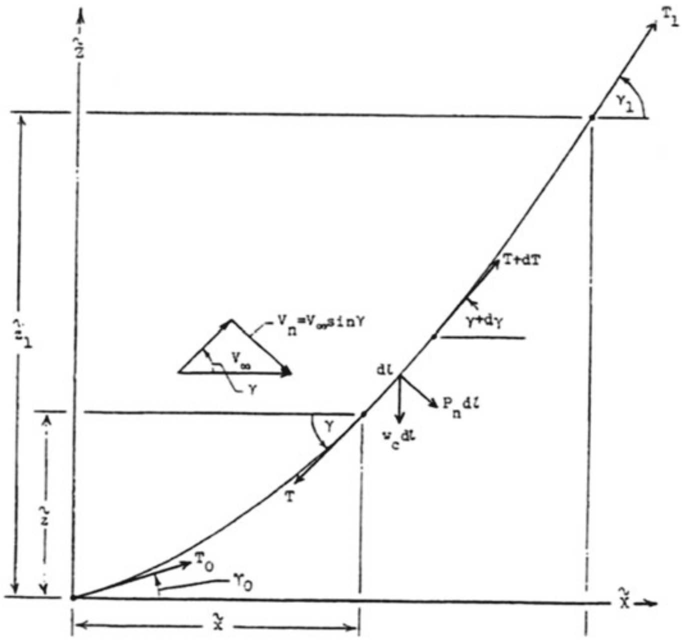

Fig. 4 Forces acting on the tether cable [8]

$$\tilde{z}_1 = \frac{T_1 - T_0}{w_c} \quad \text{where} \quad \mathrm{d}\tilde{z} = \mathrm{d}l \sin\gamma = \frac{\mathrm{d}T}{w_c} \tag{17}$$

where $\overline{\lambda}(\gamma) = \int\limits_0^\gamma \frac{\tau(\gamma)}{\left(\sin^2\gamma + 2\overline{p}\cos\gamma\right)} \mathrm{d}\gamma$ $\overline{\lambda}_0 = \overline{\lambda}(\gamma_0)$ and $\overline{\lambda}_1 = \overline{\lambda}(\gamma_1)$.

3.5 Cable Force Derivatives

Consider cable in its equilibrium position. If upper end is slowly displaced in the $\tilde{x}\tilde{z}$—plane from its original position $\tilde{x}_1, \tilde{z}_1$ to a new position the resultant x- and z-force increments are

$$\mathrm{d}F_x = k_{xx}\mathrm{d}\tilde{x} + k_{xz}\mathrm{d}\tilde{z} \tag{18a}$$

$$\mathrm{d}F_z = k_{zx}\mathrm{d}\tilde{x} + k_{zz}\mathrm{d}\tilde{z} \tag{18b}$$

The cable derivatives (spring constants) k_{xx}, k_{xz}, k_{zx} and k_{zz} for the longitudinal case can be expressed as [8]:

$$k_{xx} = \frac{1}{\delta}\left[T_1 \cos\gamma_1(\sin\gamma_1 - \sin\gamma_0) + n(z_1 - 1\sin\gamma_0)\sin^3\gamma_1\right] \tag{19a}$$

$$k_{xz} = \frac{1}{\delta}\left[T_1 \cos\gamma_1(\cos\gamma_0 - \cos\gamma_1) + n(1\cos\gamma_0 - \tilde{x}_1)\sin^3\gamma_1\right] \tag{19b}$$

$$k_{zx} = \frac{1}{\delta}\left[T_1 \sin\gamma_1(\sin\gamma_1 - \sin\gamma_0) - \left(w_c + n\sin^2\gamma_1\cos\gamma_1\right)(\tilde{z}_1 - 1\sin\gamma_0\right] \tag{19c}$$

$$k_{zz} = \frac{1}{\delta}\left[T_1 \sin\gamma_1(\cos\gamma_0 - \cos\gamma_1) - \left(w_c + n\sin^2\gamma_1\cos\gamma_1\right)(1\cos\gamma_0 - \tilde{x}_1)\right] \tag{19d}$$

where $\delta = x_1(\sin\gamma_1 - \sin\gamma_0) + z_1(\cos\gamma_0 - \cos\gamma_1) - 1\sin(\gamma_1 - \gamma_0)$.

The single lateral cable derivative determined by considering a small force dF_Y to act in the y-direction on the upper end of the cable is given by the following expression.

$$\mathrm{d}F_Y = k_{yy}\mathrm{d}y \tag{20}$$

where $k_{yy} = \frac{n\sqrt{\tau_1\left(\sin^2\gamma_1 + 2\overline{p}\cos\gamma_1\right)}}{\int_{\gamma_0}^{\gamma_1}\sqrt{\frac{\tau(\gamma)}{\left(\sin^2\gamma + 2\overline{p}\cos\gamma\right)}}\,\mathrm{d}\gamma}$.

3.6 Stability Equations (Longitudinal)

The stability equations are obtained by setting the equilibrium trim portions of the equations of motion (Eq. 10a–10f) equal to zero. The following working forms of the stability equations [3] written about the balloon center of mass are obtained.

***X*-Force**.

$$m_x\ddot{x}_e + \left[\frac{\rho V_\infty S}{2}\left(2C_D + C_{D_u}\right)\right]\dot{x}_e + k_{xx}x_e + \left[\frac{\rho V_\infty S}{2}\left(C_{D_\alpha} - C_L\right)\right]\dot{z}_e + k_{xz}z_e + \left[k_{x\theta} + \frac{\rho V_\infty^2 S C_{D_\alpha}}{2}\right]\theta = 0 \tag{21a}$$

***Z*-Force**.

$$m_z\ddot{z}_e + \frac{\rho V_\infty S}{2}\left(2C_L + C_{L_u}\right)\dot{x}_e + k_{zx}x_e + \frac{\rho V_\infty S}{2}\left(C_{L_\alpha} + C_D\right)\dot{z}_e + k_{zz}z_e + \frac{\rho V_\infty S\overline{c}}{4}\left(C_{L_{\dot{\alpha}}} + C_{L_q}\right)\dot{\theta} + \left(k_{z\theta} + \frac{\rho V_\infty^2 S C_{L_\alpha}}{2}\right)\theta = 0 \tag{21b}$$

Pitching Moment.

$$-\left[\frac{\rho V_\infty S\overline{c}}{2}\left(2C_m + C_{m_u}\right)\right]\dot{x}_e + k_{\theta x}x_e - \left[\frac{\rho S\overline{c}^2}{4}C_{m_{\dot{\alpha}}}\right]\ddot{z}_e - \left(\frac{\rho V_\infty S\overline{c}}{2}C_{m_\alpha}\right)\dot{z}_e + k_{\theta z}z_e$$
$$+ I_y\ddot{\theta} - \left[\frac{\rho V_\infty S\overline{c}^2}{4}\left(C_{m_{\dot{\alpha}}} + C_{m_q}\right)\right]\dot{\theta}$$
$$+ \left(k_{\theta\theta} + M_{s_1} - \frac{\rho V_\infty^2 S\overline{c}}{2}C_{m_\alpha}\right)\theta = 0 \tag{21c}$$

Using the mathematical model, the stability equations can be written in the state space form as given below:

$$\frac{\mathrm{d}x}{\mathrm{d}t} = Ax + Bu \tag{22}$$

where A is the characteristic matrix and B is the input matrix.

Since no control input is being used, the matrix A gives the characteristics of the aerostat system. The equation for longitudinal and lateral stability case can be expressed in the following matrix form, respectively.

$$\begin{bmatrix} \dot{u} \\ \dot{w} \\ \dot{q} \\ \dot{\theta} \\ \dot{x} \\ \dot{z} \end{bmatrix} = A \begin{bmatrix} u \\ w \\ q \\ \theta \\ x \\ z \end{bmatrix} \tag{23}$$

The roots of characteristic equation obtained by computing stability matrix A for longitudinal and lateral case give an insight into the stability of the system.

4 Effect of Geometrical Parameters on Longitudinal Stability Boundaries

The computed values of longitudinal frequencies (ω) and damping rates (η) for the considered aerostat have been plotted as a function of wind velocity in Fig. 5a, b and in root locus form in Fig. 5c. Figure 5a, b indicates that the considered aerostat has three oscillatory modes of motion for the given range of the wind velocities. It can be observed from Fig. 5b that the aerostat was longitudinally stable except below wind velocity of 2 m/s at which one of the roots becomes positive. This fact is also evident from the negative slope of the plot between pitching moment coefficient and angle of attack as shown in Fig. 5d. It could also be observed from Fig. 5b that mode 2 splits into two real non-oscillatory modes above wind velocity of 19 m/s and again merged into one at 35 m/s.

Fig. 5 **a** Variation of ω with V for longitudinal case. **b** Variation of η with V for longitudinal case. **c** ω versus η (Root locus plot for longitudinal case). **d** C_m versus α for longitudinal case

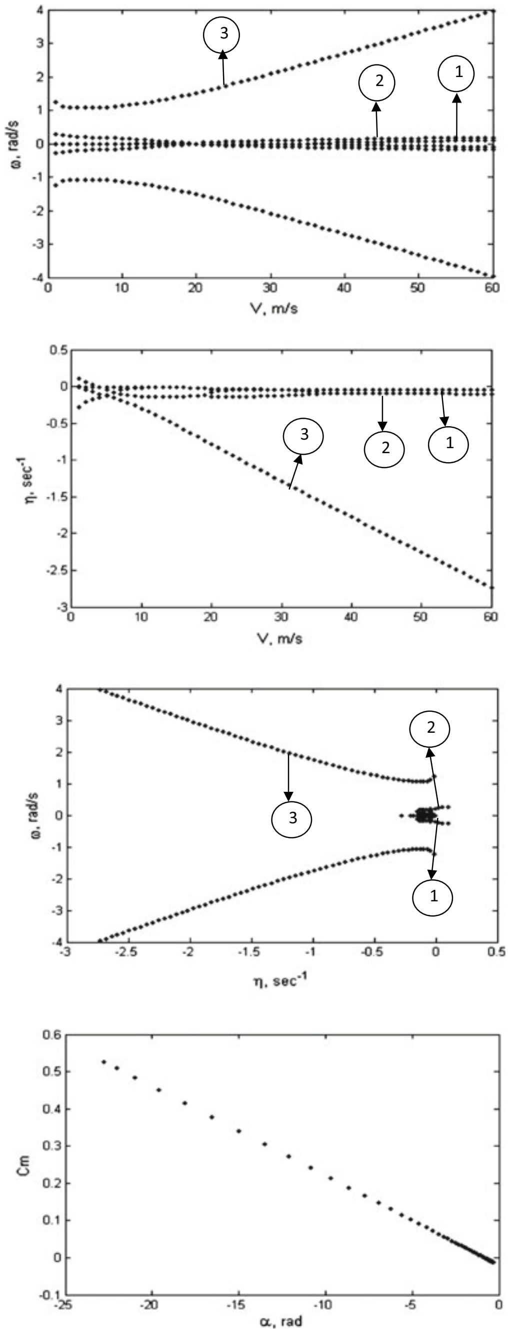

Next, geometrical parameters were varied to see the effect on longitudinal stability boundaries of the considered aerostat. The results showing the effect of different parameters on the stability boundaries for a range of speed have been presented in the graphical form. Figures 6, 7, 8, 9, 10, 11, 12 and 13 show that the aerostat is unstable below the speed of 2 m/sec and in the region bounded by the two curved/straight boundaries. The unstable region increases or decreases with increase or decrease in the values of most of the dimensional parameters of the considered aerostat. Very little or negligible effect on stability boundaries was observed for some parameters.

It can be observed from Figs. 6, 7, 8, 9, 10, 11, 12 and 13 that the parameters such as L_{tr}, T_{tr}, L_{br}, L_{sr}, C.G. (moment arm), l, d_c, w_c affect the stability boundaries strongly while the parameters such as L_{cg}, H_{cg}, H_{br} and H_{sr} have very little or negligible effect on the stability characteristics/boundaries of the aerostat. It can be observed that the decrease in L_{tr} (the horizontal component of distance between RP and BCP) decreases the unstable region while decrease in T_{tr} (the vertical component of distance between RP and BCP) increases the unstable region (Fig. 6a, b). The change in horizontal (L_{cg}) or vertical (H_{cg}) component of distance from RP to COM has very little or negligible effect on the stability boundaries (Fig. 7a, b). Increase in the value of horizontal component of distance from RP to COB (L_{br}) and COM

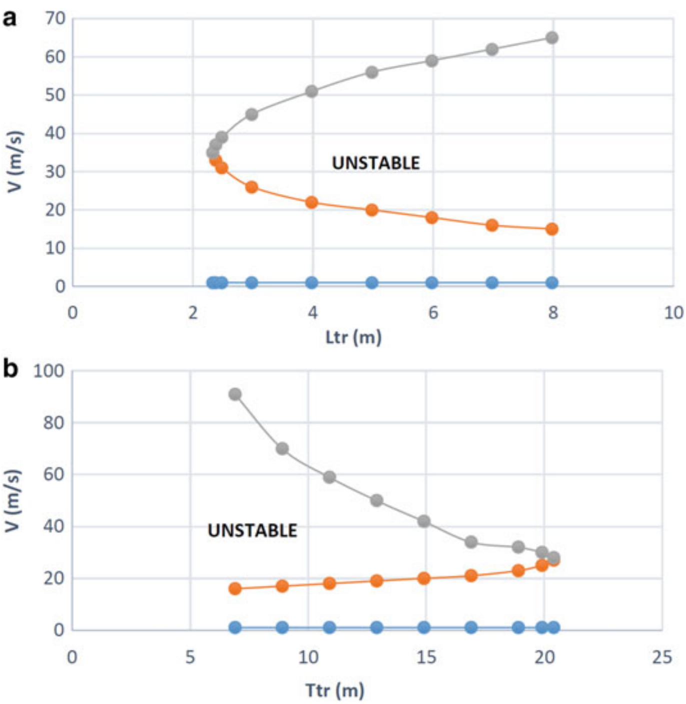

Fig. 6 **a** Effect of L_{tr} on longitudinal stability boundary **b** Effect of T_{tr} on longitudinal stability boundary

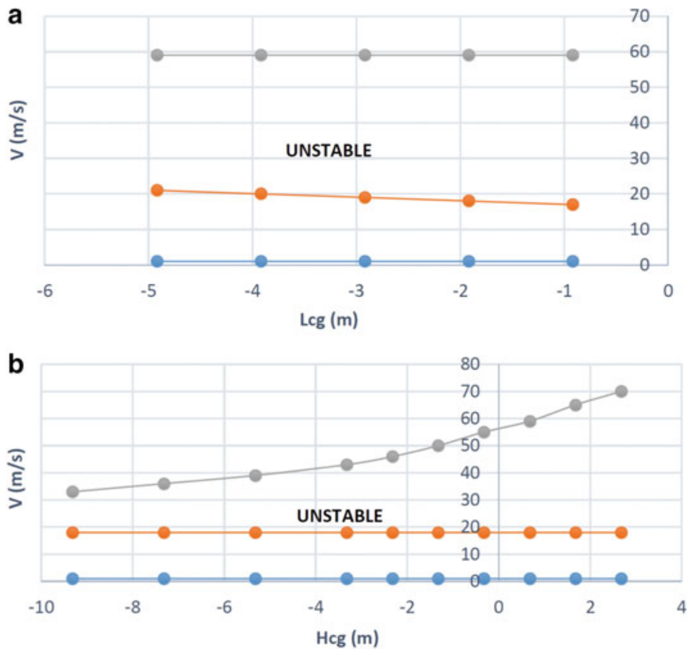

Fig. 7 **a** Effect of L_{cg} on longitudinal stability boundary **b** Effect of H_{cg} on longitudinal stability boundary

of structure (L_{sr}) decreases the unstable regions while the vertical components (H_{br} and H_{sr}) have negligible effect (Figs. 8a, b and 9a, b).

Reduction in tether cable length (l), cable diameter (d_c) and cable weight (w_c) leads to the reduction in the unstable region (Figs. 10, 11 and 12). Increase in the horizontal tail moment arm reduces the unstable region (Fig. 13).

5 Conclusion

Longitudinal stability analysis and effect of variation of geometrical parameters on longitudinal stability boundaries for a balloon tethered in a steady wind has been presented. Equations of motion of the considered aerostat included aerodynamic, tether cable, buoyancy and gravity forces along with aerodynamic apparent mass and structural mass terms. After mathematical modeling, the roots of the characteristic stability equation were computed and plotted for various steady-wind conditions. It was observed from graphical presentations that the considered aerostat was stable longitudinally. Later on, parametric trend study was carried out to show the influence of various dimensional and aerodynamic parameters of aerostat on longitudinal stability boundaries for a wide range of steady-wind speeds. The study suggests that

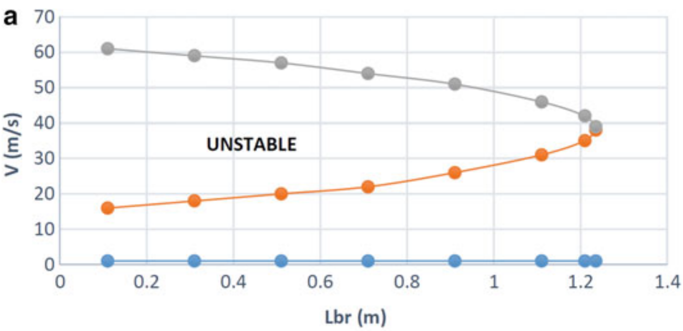

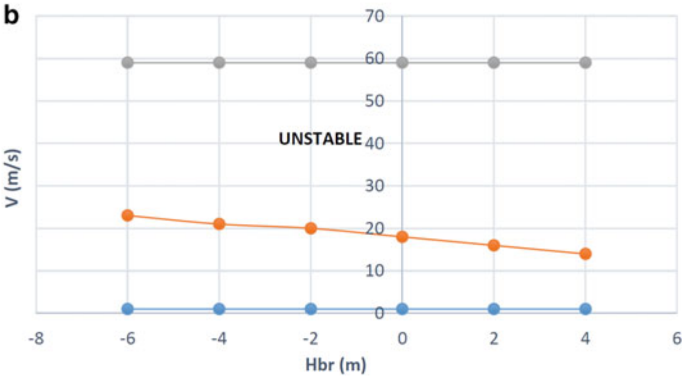

Fig. 8 **a** Effect of L_{br} on longitudinal stability boundary **b** Effect of H_{br} on longitudinal stability boundary

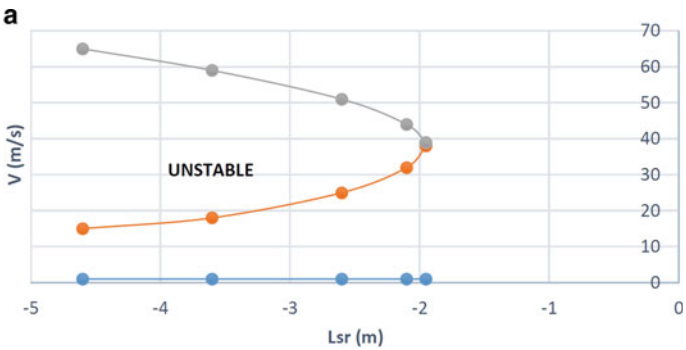

Fig. 9 **a** Effect of L_{sr} on longitudinal stability boundary **b** Effect of H_{sr} on longitudinal stability boundary

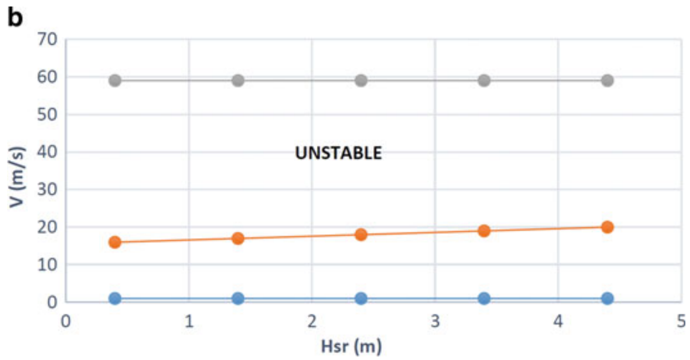

Fig. 9 (continued)

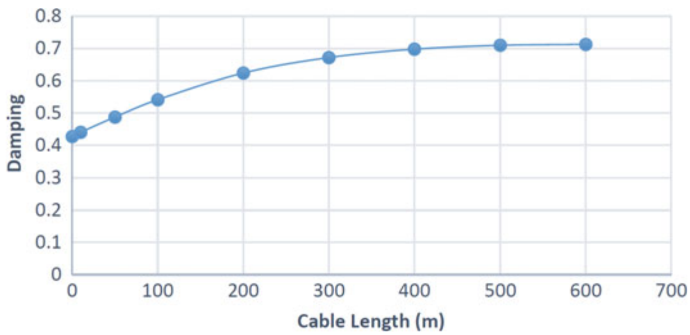

Fig. 10 Effect of cable length (m) on longitudinal stability

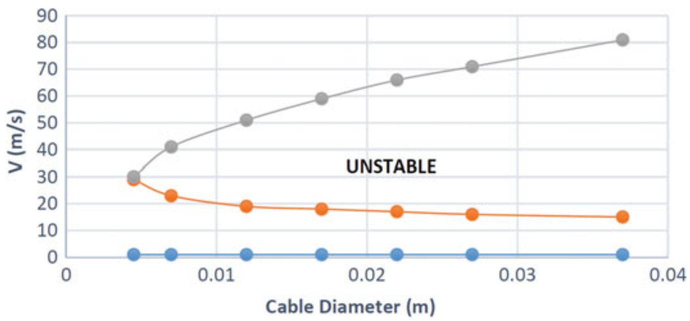

Fig. 11 Effect of cable diameter (d_c) on longitudinal stability boundary

the judicious and feasible choice of various geometrical parameters can be utilized to design a new tethered aerostat which can remain stable for a wide range of wind speeds. The limitation of the stability analysis carried out was that the downwash has been neglected and provides the basis for the future scope.

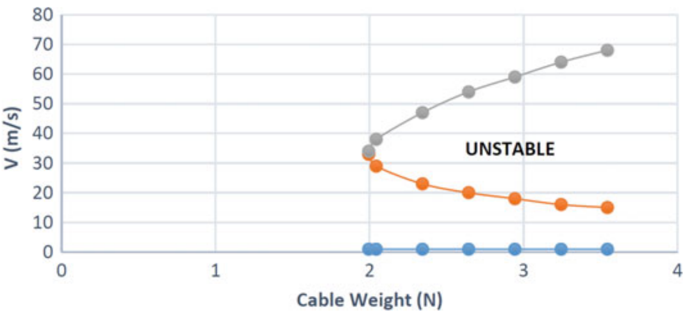

Fig. 12 Effect of cable weight (w_c) on longitudinal stability boundary

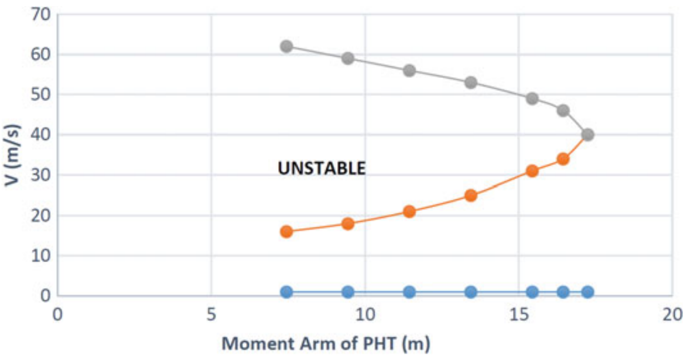

Fig. 13 Effect of moment arm (PHT) on longitudinal stability boundary

References

1. Gupta P, Pant RS (Dec 2005) A methodology for initial sizing and conceptual design studies of an aerostat, international seminar on challenges on aviation technology, integration and operations (CATIO-05), technical. Sessions of 57th annual general meeting of aeronautical society of India
2. Gawande VN, Bilaye P, Gawale AC, Pant RS, Desai UB (Sept 2007) Design and fabrication of an aerostat for wireless communication in remote areas. System technology conference, Belfast, Northern Ireland, UK
3. Raina AA, Bhandari KM, Pant RS (6–10 April 2009) Conceptual design of a high altitude aerostat for study of snow patterns. Proceedings of international symposium on snow and avalanches (ISSA-09), SASE, Manali, India
4. Rajani A, Pant RS, Sudhakar K (4–7 May 2009) Dynamic stability analysis of a tethered aerostat. Proceedings of 18th AIAA lighter-than-air system technology conference, seattle, Washington, USA
5. Rajani A, Pant RS, Sudhakar K (Sept–Oct 2010) Dynamic stability analysis of a tethered aerostat. J Aircraft 47(5)
6. Redd LT, Benett RM, Bland SR (Sept 1972) Analytical and experimental investigation of stability parameters for a balloon tethered in wind, 7th AF cambridge research laboratories scientific balloon symposium. Portsmouth, N.H.

7. Redd LT, Benett RM, Bland SR (1973) Experimental and analytical determination of stability parameters for a balloon tethered in wind, numeric value TD D-2021
8. Redd, L.T., Benett, R.M. and Bland, S.R., "Stability Analysis and Trend Study of a Balloon Tethered in Wind, with Comparisons", NASA TN D-7272, October, 1973.
9. Srivastava S (April 2009) Stability analysis and parameter trend study of single tether aerostats. M. Tech thesis, DAE, IIT, Kanpur
10. Rakesh K et al (2011) Parametric trend study during stability analysis of a tethered aerostat. J Aerospace Sci Technol 63(2)
11. Khouri GA, Gillett JD (1999) Airship technology. Cambridge University Press, UK
12. Delaurier JD (1972) A stability analysis for tethered aerodynamically shaped balloons. J Aircr 9(9):646–651
13. Lambert C, Nahon M (July–Aug 2003) Stability analysis of a tethered aerostat. J Aircraft 40(4)
14. Li Y, Nahon M (Nov–Dec 2007) Modeling and simulation of airship dynamics. J Guidance, Control Dyn 30(6)
15. Neumark S (1963) Equilibrium configurations of flying cables of captive balloons and cable derivatives for stability calculations, R & M no. 3333, Brit., A.R.C.
16. Delaurier JD (Dec 1970) A first order theory for predicting the stability of cable towed and tethered bodies where the cable has a general curvature and tension variation, VKI-TN-68, Von Karman Institute of Fluid Dynamics
17. Delaurier JD (1972) A stability analysis of cable-body system totally immersed in fluid stream. Numeric Value CR-2021
18. Raymer DP (2006) Aircraft design: a conceptual approach, 4th edn. AIAA Education Series, New York, NY
19. Etkin B, Lloyd DR (1996) Dynamics of flight: stability and control, 3rd edn. Wiley
20. Nelson RC. Flight stability and automatic control, 2nd edn. McGraw-Hill, 98